Supporting Information

Klein et al. 10.1073/pnas.1416212112

SI Experimental Procedures

Spatial Temperature Gradient. The linear temperature gradient was constructed from custom-machined aluminum and steel sheets and blocks. The top plate (61 × 30 × 0.64 cm) of black anodized aluminum bridged across the hot and cold aluminum reservoir blocks (10 × 30 × 3.8 cm), with thin steel diffuser plates (10 × 30 × 0.16 cm) inserted between the top plate and the blocks to improve spatial uniformity. Thermal compound provided thermal contact between the parts. Navigating larvae crawled on a 22- × 22-cm surface of 1% LB agar atop a thin anodized aluminum plate (22 × 22 × 0.16 cm). Glycerol was used to improve thermal contact between the top plate and the thin plate with the gel.

The cold reservoir temperature was maintained with a PID (proportional-integral-derivative) controller and H-bridge amplifier (Accuthermo), powered by a switching supply (Oven Industries) driving a thermoelectric cooler (TEC; Ferrotec) that pumped heat between the reservoir block and a liquid-cooled waterblock (Swiftech); the liquid was circulated with a pump and chiller unit (VWR). The hot reservoir was also controlled with PID feedback (Newport Electronics) that delivered ac voltage via a solid-state relay (Omega) to four resistive cartridge heaters (McMaster-Carr) embedded in the reservoir block. The resistance temperature detectors (McMaster-Carr) used for both PID feedback loops were secured to the top plate near each reservoir block. Temperature at the agar gel surface was measured with a type T thermocouple probe (Physitemp) before and after each experiment to check for thermal drift; the same probe was used to systematically measure temperature in both horizontal dimensions on the surface. Temperature was found to be constant in the direction perpendicular to the gradient.

Thermal Fluctuation Apparatus. The stage for analyzing behavior in response to random thermal flicker was constructed from a custom-machined copper plate (13.3 × 13.3 × 0.64 cm), spray-painted black to improve image contrast. Larvae crawled inside a 12.1- × 12.1-cm pocket cut 0.40 cm deep, atop a very thin (300 μm) layer of 3% LB agar. Temperature control was established with a PID system similar to the spatial gradient apparatus, but with four identical TECs (Custom Thermoelectrics) arranged in a symmetric square pattern underneath the copper plate. The PID feedback temperature sensor was clamped gently to the agar surface near one corner. These implements resulted in a spatially uniform, temporally varying temperature stimulus for crawling larvae, which was confirmed by using a thermal imaging camera. Temperatures were selected at random in a 16–18 °C range, with values updated every 0.125 s, then filtered in frequency space to ensure that all temporal gradients up to 1 °C/s were uniformly represented.

Optogenetic Activation Apparatus. The stage for analyzing behavior in response to random LED light flicker was an aluminum platform with a 2% agar gel ∼4 mm thick. Light for optogenetic activation of the channelrhodopsin CsChrimson was delivered from a 39- × 39-cm grid of red (624 nm) LEDs positioned above the crawling larvae at the same height as the camera. The light intensity was randomly assigned as on or off at each 0.25-s interval during recording.

Behavior Data Analysis. Larval crawling images were processed by using the MAGAT Analyzer software (1), which determines the position and contour of each larva to form tracks that are broken down into runs and turns (Fig. 1*A*). Turning behavior and navigational preference index were calculated by using custom scripts written in MATLAB (Mathworks); turning rate is defined as the number of turns divided by the elapsed time during runs, and the navigational preference index is the average component of velocity during runs parallel to the gradient and toward the warm side, averaged for all larvae in each experiment, divided by the mean crawling speed during runs: preference index = $\langle v_x \rangle / \langle v \rangle$.

Tracks were also filtered by speed, duration, displacement, and crawling direction (forward vs. backward). Thus, shorter tracks are ignored in navigation analysis and the construction of reverse correlation filters. This ensures that only bouts of several minutes of uninterrupted crawling are counted (i.e., with no collisions or direct interaction with other larvae), which allows us to record the activity of many larvae simultaneously without significant interaction between animals.

To calculate the statistics in Fig. 1, the temporal gradient experienced by each larva preceding each turn was calculated by using crawling direction, speed, and the direction and steepness of the spatial temperature gradient during the run that preceded the turn. Turn rate (Fig. 1*D*) was calculated by using a linear regression of run duration vs. speed (speed and run direction were uncorrelated). Temporal gradients experienced by each larva during each head sweep were calculated by using the vector displacement of the head during each head sweep, the duration of the head sweep, and the direction and steepness of the ambient spatial temperature gradient. Run duration, turn size, and the probability of starting a new run during each head sweep were calculated for each temporal gradient bin by using custom scripts in MATLAB and Igor Pro.

In Vivo Imaging. Larvae were imaged on a custom-built temperature control stage, where a PID controller and H-bridge amplifier (Accuthermo) drove a TEC (Newark) that pumped heat into and out of a thin copper plate (7.4 × 7.4 × 0.5 cm), with a liquid-cooled water block (Swiftech) acting as a thermal reservoir. A type-T thermocouple microprobe (Physitemp) was placed on the copper plate underneath a thin steel tab (7.4 × 2.5 × 0.013 cm) (Fig. 4*A*).

After rinsing in distilled water, larvae were placed on the steel tab directly above the temperature probe and held in place with downward force from a glass coverslip secured to a 1.6-mm-thick aluminum frame. The frame was attached to a vertical translation mount (Newport), allowing for precision control of the coverslip position.

Temperature was delivered by altering the PID controller's set point dynamically, using custom software written in LabVIEW (National Instruments). Because the temperature at the position of the larva could differ from the embedded thermocouple probe temperature, larval temperature was calibrated by using a second probe taking the larva's place while delivering the same temperature programs. Random thermal flicker for calcium imaging was generated in the same way as for sine-wave and ramps, with two exceptions: The thermocouple probe was placed directly beneath the larva and separated by a thin layer of polymide tape; and a 40× air objective was used to avoid thermal sinking to the objective during imaging.

The microscope objective was mounted on a piezoelectric transducer (Physica Instrumente). The objective position was corrected based on the temperature measured by the thermocouple probe, compensating for thermal expansion and contraction in the temperature control stage (e.g., see Fig. S1*C*, *Inset*). This minimized image defocusing due to temperature changes,

and temperature could be varied by >30 °C without significantly altering the image focus.

Images from an EM CCD camera (Andor Technology) were recorded by using either iQ (Andor Technology) or NIS Elements (Nikon Instruments) software. Calcium and voltage signal analyses were performed by using custom software written in Igor Pro (Wavemetrics). Ellipsoid volumes were drawn around each neuron of interest, and for each 3D image stack, the brightest 100 pixels in the volume were averaged to generate the raw signal. $\Delta F/F$ was then computed, with F set as the initial signal level of the neuron before temperature change. Subtracted background levels were determined by using a nearby ellipsoid volume not containing any fluorescent neurons.

1. Gershow M, et al. (2012) Controlling airborne cues to study small animal navigation. *Nat Methods* 9(3):290–296.

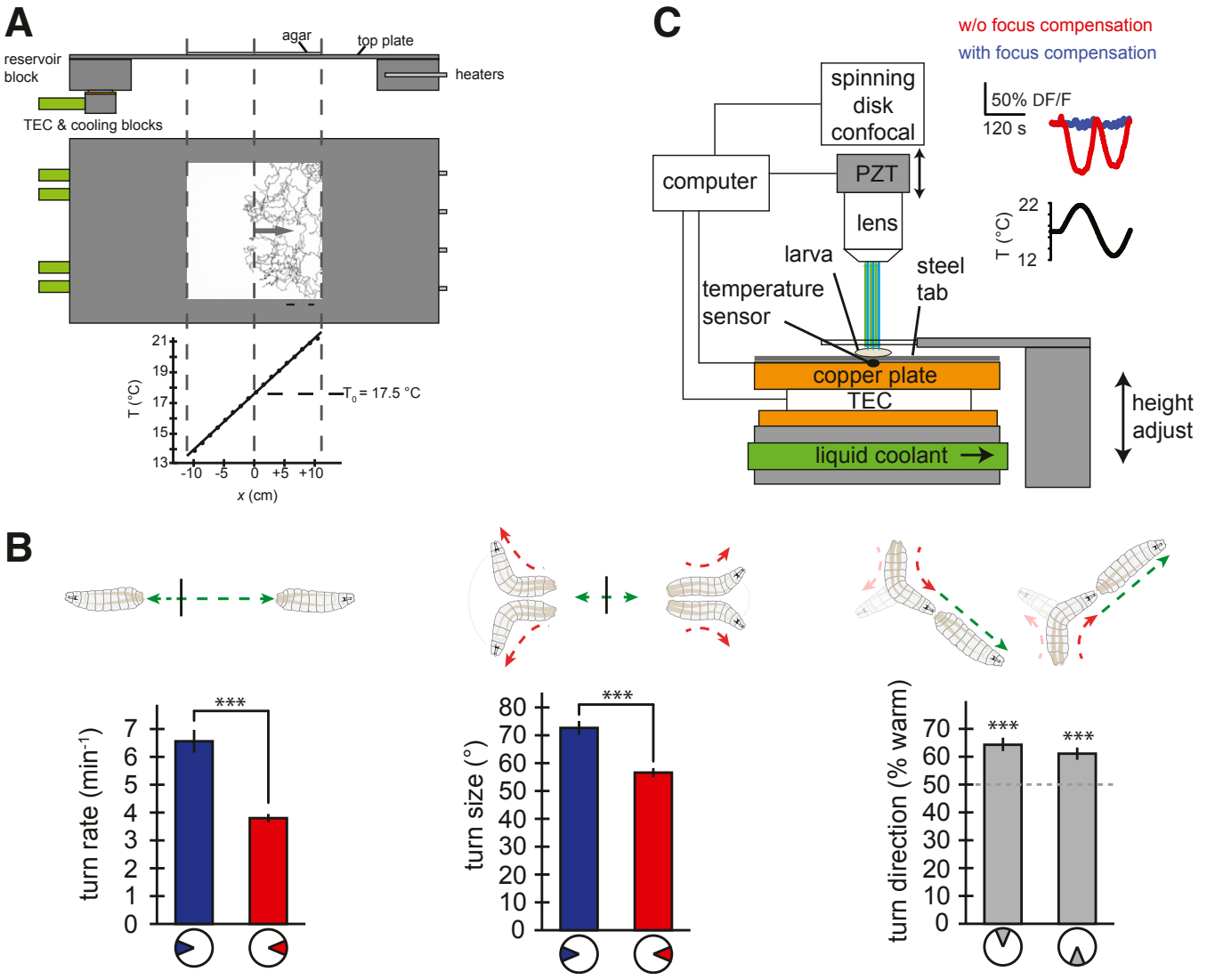

Fig. S1. (*A*) Schematic of the spatial temperature gradient apparatus, with stable cold and warm sides maintained to establish a linear gradient across the surface of an agar gel. Trajectories from 22 larvae are superimposed onto the aerial view, where larvae starting at 17.5 °C crawl to the warm side of a linear gradient that was measured directly on the agar surface by using a thermocouple. Drawing is to scale. (*B*) Statistics of run-and-turn movements reveal the key biases that drive movement up gradients illustrated above each graph. (*B*, *Left* and *Center*) Larvae have a higher average turn rate (*Left*) and larger turn size (*Center*) when the run preceding each turn is selected from the octile of angles pointed toward colder temperatures than the octile toward warmer temperatures. (*B*, *Right*) Larvae tend to start new runs toward warmer temperatures after runs pointed orthogonal to the gradient. Statistics were calculated from the trajectories of 85 wild-type larvae segmented into 3,642 runs. Error bars are ± SEM. ***$P < 0.001$ (Mann–Whitney–Wilcoxon test for turn rate; Student's t test for turn size and direction). (*C*) Schematic of spatial temperature gradient apparatus, with stable cold and warm sides (*Top*) maintained to establish a linear gradient across the surface of an agar gel. Trajectories from 22 larvae are superimposed onto the aerial view (*Middle*), where larvae starting at 17.5 °C crawl to the warm side of a linear gradient that was measured directly on the agar surface using a thermocouple (*Bottom*). Drawing is to scale.

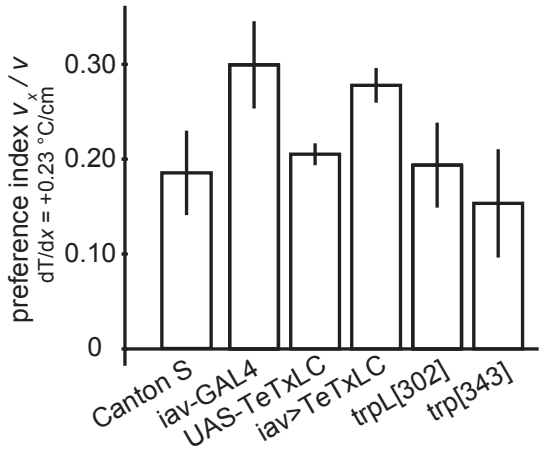

Fig. S2. Navigation up temperature gradients quantified for wild-type and mutant second-instar larvae in the same way as shown in Fig. 1*B*. Larvae with *inactive* neurons silenced by tetanus toxin light chain perform cool avoidance as well as their parent strain controls. *trpL[302]* mutants and *trp[343]* mutants also perform cool avoidance as well as wild-type larvae. Each measurement represents trajectories from at least 96 larvae. Error bars are ± SEM.

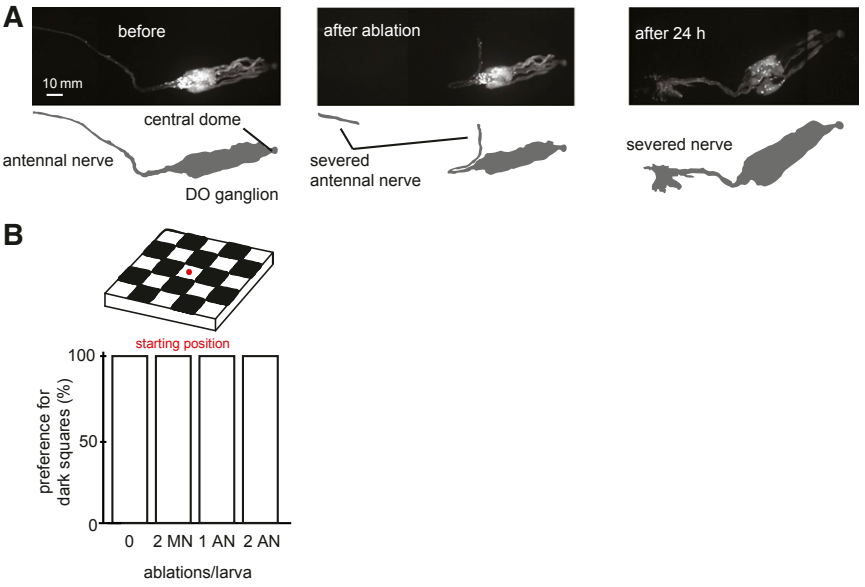

Fig. S3. (*A*) Images and silhouettes of laser ablation of the antennal nerve between the dorsal organ and the central brain in a first instar *Orco-RFP; UAS-mCD8::GFP* larva: before ablation (*Left*), immediately after ablation (*Center*), and 24 h later (*Right*). (*B*) The ablated larvae used in Fig. 3*B* perform phototaxis on a checkerboard pattern of light and dark squares. (*B*, *Upper*) Schematic representation of the light environment, where each larva begins in a light square and crawls into dark squares. (*B*, *Lower*) Histogram shows the percentage of times that the larvae moved toward the dark square when it encountered boundaries between the light and dark squares.

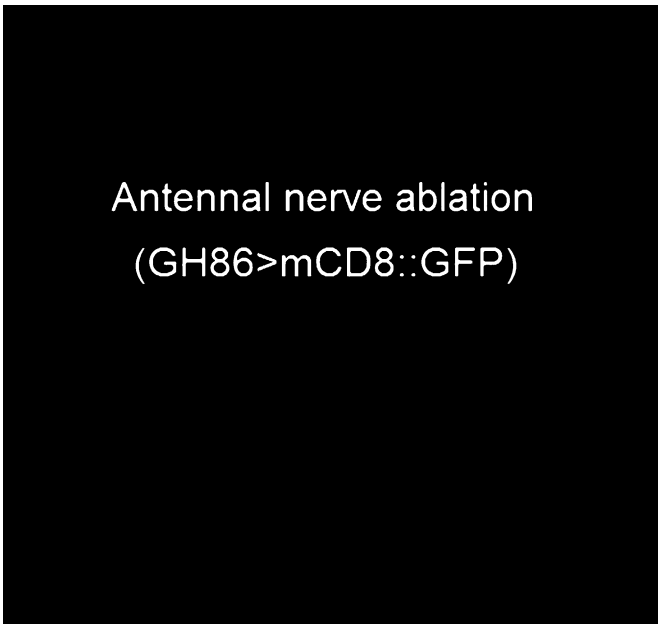

Movie S1. Calcium response in *NP4486* > *GCaMP3* larvae subjected to sinusoidal and linear temperature waveforms. The three thermosensory neurons (A-type medial, blue; A-type lateral, green; B-type, red) show increased activity during cooling, with distinct timing and thresholds between A and B types. Movies are a sequence of maximum intensity z-projections of 3D confocal stacks.

Movie S1

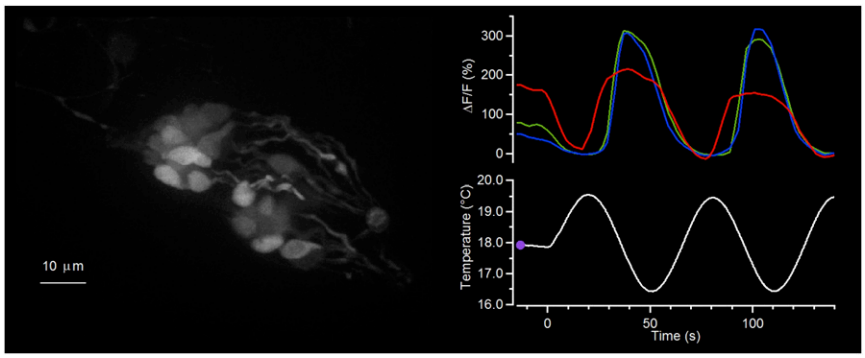

Movie S2. Thermosensory neurons in the DOG exhibit morphology distinct from surrounding ORNs. First part: the DOG in a *GH86* > *mCD8::GFP* larva. Second part: left and right DOG in an *R11F02* > *mCD8::GFP* larva.

Movie S2

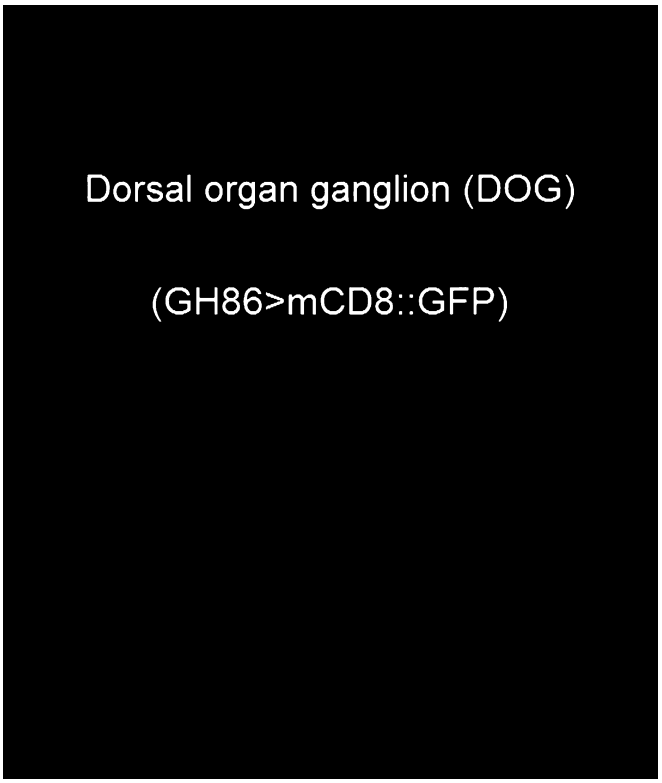

Movie S3. Laser ablation of antennal and maxillary nerves. First part: single-plane confocal images of an immobilized larva subjected to laser ablation that severs its antennal nerve, which connects the DOG to the central brain. Second part: similar images for a larva subjected to laser ablation of its maxillary nerve, which connects the TOG to the central brain. Third part: similar images for a larva reimmobilized 24 h after both antennal nerves were severed under laser ablation; the axon bundles have failed to regrow.

Movie S3

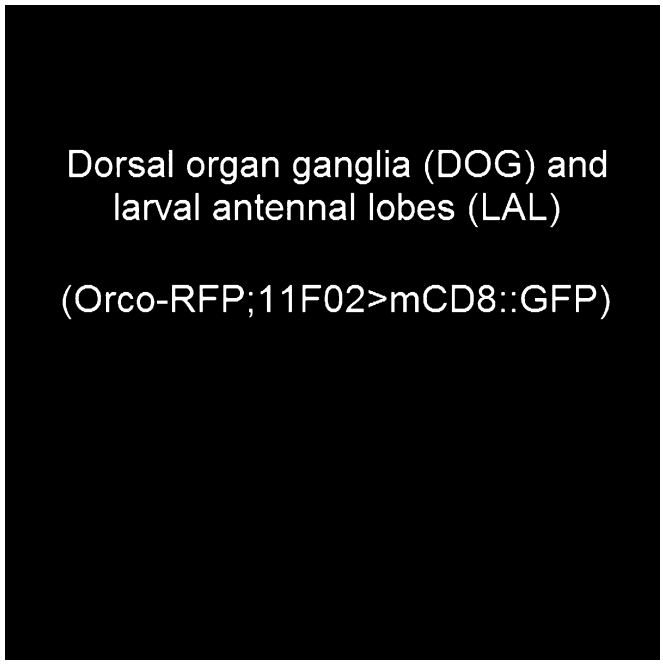

Movie S4. DOG thermosensory neurons are not ORNs. A *Orco-RFP;R11F02* > *MCD8::GFP* larva immobilized and imaged with a 3D confocal microscope. First part: whole larva showing both the DOG and LAL regions. Second part: rotating 3D image of the two DOGs. Third part: rotating 3D image of both halves of the LAL.

Movie S4